

Article

# Boosting Hydrogen Production from Formic Acid over Pd Catalysts by Deposition of N-Containing Precursors on the Carbon Support

Fedor S. Golub <sup>1,2</sup>, Sergey Beloshapkin <sup>3</sup>, Artem V. Gusel'nikov <sup>4</sup>, Vasily A. Bolotov <sup>1</sup>,  
Valentin N. Parmon <sup>1,2</sup> and Dmitri A. Bulushev <sup>1,2,\*</sup> 

<sup>1</sup> Laboratory of Catalytic Methods of Solar Energy Transformation, Boreskov Institute of Catalysis, SB RAS, 630090 Novosibirsk, Russia; fedorglb@gmail.com (F.S.G.); bolotov@catalysis.ru (V.A.B.); parmon@catalysis.ru (V.N.P.)

<sup>2</sup> Department of Natural Sciences, Novosibirsk State University, 630090 Novosibirsk, Russia

<sup>3</sup> Bernal Institute, University of Limerick, V94 T9PX Limerick, Ireland; serguei.belochapkin@ul.ie

<sup>4</sup> Laboratory of Physico-Chemistry of Nanomaterials, Nikolaev Institute of Inorganic Chemistry, SB RAS, 630090 Novosibirsk, Russia; artemg@ngs.ru

\* Correspondence: dmitri.bulushev@catalysis.ru

Received: 18 September 2019; Accepted: 11 October 2019; Published: 14 October 2019



**Abstract:** Formic acid is a promising liquid organic hydrogen carrier (LOHC) since it has relatively high hydrogen content (4.4 wt%), low inflammability, low toxicity and can be obtained from biomass or from CO<sub>2</sub>. The aim of the present research was the creation of efficient 1 wt% Pd catalysts supported on mesoporous graphitic carbon (Sibunit) for the hydrogen production from gas-phase formic acid. For this purpose, the carbon support was modified by pyrolysis of deposited precursors containing pyridinic nitrogen such as melamine (Mel), 2,2'-bipyridine (Bpy) or 1,10-phenanthroline (Phen) at 673 K. The following activity trend of the catalysts Pd/Mel/C > Pd/C ~ Pd/Bpy/C > Pd/Phen/C was obtained. The activity of the Pd/Mel/C catalyst was by a factor of 4 higher than the activity of the Pd/C catalyst at about 373 K and the apparent activation energy was significantly lower than those for the other catalysts (32 vs. 42–46 kJ/mol). The high activity of the melamine-based samples was explained by a high dispersion of Pd nanoparticles (~2 nm, HRTEM) and their strong electron-deficient character (XPS) provided by interaction of Pd with pyridinic nitrogen species of the support. The presented results can be used for the development of supported Pd catalysts for hydrogen production from different liquid organic hydrogen carriers.

**Keywords:** hydrogen production; formic acid decomposition; Pd/C; melamine; g-C<sub>3</sub>N<sub>4</sub>; bipyridine; phenanthroline; N-doped carbon

## 1. Introduction

According to research performed for the US Department of Energy [1], it is expected that despite growth in non-fossil fuel consumption will be greater than that of fossil fuels, the fossil fuels will still account for 78% of energy use in 2040. The resulting problems are obvious. Among them are reducing non-renewable sources of energy and high CO<sub>2</sub> emission, which are suspected to excite global warming with all related problems. For this reason, interest in eco-friendly and renewable sources like hydrogen, water, solar or wind energy grows every year.

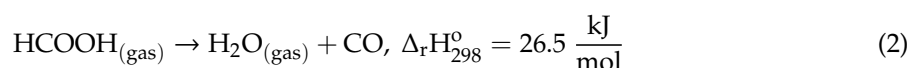
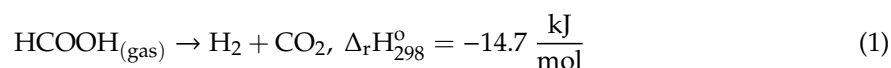
Hydrogen is a perspective fuel due to possibility of its applications including fuel cells. The main problems with the hydrogen use are its storage and transportation. The various methods based on physical or chemical storage have been developed to solve these problems. The physical methods assume storage of molecular hydrogen in vessels at high pressure and low temperatures or

hydrogen adsorption on high surface area materials like porous carbon. However, both these methods lead to large energy losses; therefore, such storage may appear inefficient. The chemical method implies hydrogen storage in a chemical bounded form, in molecules with high hydrogen content. This hydrogen can be efficiently recovered by a catalytic or non-catalytic reaction.

At the present time, formic acid is considered as an efficient liquid organic hydrogen carrier (LOHC) [2]. It has sufficiently good physical properties such as stability under standard conditions, low inflammability, low toxicity (compared to methanol, ammonia or hydrazine, for example), and relatively high hydrogen content (4.4 wt%). It is important to note, that the density of gravimetric energy of formic acid is seven times higher than that of the currently used lithium-ion batteries [3]. In addition, formic acid can be obtained from biomass [4,5] or from CO<sub>2</sub> and renewable H<sub>2</sub> [6].

A lot of studies related to reversible chemical hydrogen storage [7,8] provide access to potentially inexpensive, highly efficient and rechargeable hydrogen fuel cells. It is safer to use an easily decomposable hydrogen-containing material such as formic acid instead of storage and transportation of molecular hydrogen.

The catalytic formic acid decomposition reaction can be performed either in liquid phase or in gas phase. The liquid-phase decomposition is only rarely performed continuously and the determined reaction rates in this case often correspond to the initial rates and not to the steady-state. Gas-phase formic acid decomposition follows two possible pathways: through dehydrogenation to form H<sub>2</sub> and CO<sub>2</sub> (Equation (1)) and through dehydration to form CO and H<sub>2</sub>O (Equation (2)):



Depending on the catalysts and conditions the products of the Reactions (1) and (2) can transform into each other via the Water-Gas Shift or Reverse Water-Gas Shift Reactions. Only the catalysts providing very high selectivity towards Reaction (1) allow using formic acid and CO<sub>2</sub> cycle for a hydrogen storage system.

Catalysts containing no Pt-group metals [9,10] do not show promising properties as the catalysts with precious metals. Catalysts consisting of supported highly dispersed Pd particles [2,11,12] or even single Pd atoms [13–15] are often considered as the most efficient for the hydrogen production from formic acid. High dispersion of Pd implies high sensitivity of the metal properties to the support material. Flat graphitic carbon surfaces normally only weakly interact with Pd leading to agglomeration of metal and catalyst deactivation during the reaction. The approach to solving this problem is modifying the carbon surface by using other chemical elements. Modifying the surface by electron-rich nitrogen atoms increases the basicity of the support [16,17], sometimes leads to a higher dispersion of supported metal [10,17] and may change the nature of the active site. Recently, we have shown [15] for the gas phase formic acid decomposition, while Bi et al. [18] have reported for the liquid phase one that the pyridinic nitrogen sites present on the surface of carbon support can strongly interact with Pd and change its electronic state providing high activity in the reaction.

Introducing of pyridinic nitrogen on the surface of carbon support can be done by deposition of substances with pyridinic nitrogen [19–22]. This approach provides some advantages, as compared to direct synthesis of a CN material by chemical vapor deposition (CVD). The main advantage is a possibility to reach a high yield of N-containing material without a catalyst normally needed for the direct synthesis. In the latter case, the productivity of the catalyst is limited due to the blockage of the catalyst used for the CN material growth by carbon and complete deactivation. Therefore, the goal of the present work was the creation of efficient Pd catalysts for the hydrogen production from formic acid based on the N-doped carbon supports obtained by deposition of melamine, 1,10-phenanthroline and 2,2'-bipyridine on a mesoporous graphitic carbon. The choice of these N-containing precursors is explained by the presence of neighboring nitrogen atoms in their molecules. As we have shown

earlier [14,15,23] the structure of the active site on the N-doped carbon may involve a Pd atom attached to a pair of pyridinic nitrogen atoms in the armchair position on the graphene edge. This armchair unit is present in the initial molecules of 2,2'-bipyridine and 1,10-phenanthroline and could be created during pyrolysis of melamine supported on carbon.

For comparisons a graphitic carbon nitride ( $g\text{-C}_3\text{N}_4$ ) was also used as a support since it also possesses pyridinic nitrogen sites. Lee et al. [24] showed that catalysts comprising of Pd supported on graphitic carbon nitride ( $g\text{-C}_3\text{N}_4$ ) were promising for liquid phase formic acid decomposition. Additionally, Oh [25] demonstrated that this type of catalysts may produce hydrogen from liquid formic acid continuously at least within 3 h, and this result can be used for development of fuel cells.

## 2. Materials and Methods

### 2.1. Synthesis of Supports

#### 2.1.1. $g\text{-C}_3\text{N}_4$

$g\text{-C}_3\text{N}_4$  was prepared according to the procedure described by Tahir et al. [26]. This was chosen because of the reported high BET surface area of the obtained material. Nitric acid (180 mL, 0.2 M, NAK Azot, Novomoskovsk, Russia) was added to a mixture of melamine (3 g, Sigma-Aldrich, St. Louis, MO, USA) and ethylene glycol (60 mL, Acros Organics, Waltham, MA, USA) and stirred for 10 min until a white powder was precipitated. Then, the precipitate was washed with isopropyl alcohol and dried at 363 K. This sample was called Inter- $\text{C}_x\text{N}_y$ . To obtain  $g\text{-C}_3\text{N}_4$ , the Inter- $\text{C}_x\text{N}_y$  sample was heated in air in an already heated muffle furnace at 673 K for 15 min. Other heating modes were also used. It should be mentioned that melamine is inexpensive and low toxic substance [27].

#### 2.1.2. Mel/C

The used approach of doping the carbon material by substances containing pyridinic nitrogen is shown in Figure 1. Melamine (0.75 g) was mixed with isopropyl alcohol (about 100 mL) at 343 K under constant stirring. Then, the mixture was added to the mesoporous graphitic carbon—Sibunit (1.5 g, Sibunit #6, Omsk, Russia). The obtained material was kept for 10 min while isopropyl alcohol was evaporating. Then, the sample was dried at 357 K and pyrolyzed in the muffle furnace (673 K, 1 K/min) in air for 2 h. This catalyst support was called Mel/C (muf). The used Sibunit carbon is known to possess high surface area and high mechanical strength [28].

Another preparation method of the support was heating of a mechanical mixture of melamine and Sibunit (1:2) under microwave (MW) radiation in air. Microwave treatment of the mixture was carried out using a specially developed equipment (operating frequency  $2470 \pm 10$  MHz, power up to 1 kW) based on a rectangular single-mode cavity with high Q-factor ( $\sim 6000$ ), which is excited by  $\text{TE}_{102}$  oscillation mode, described in [29]. Processing MW conditions were the following:  $T = 673$  K; heating rate  $-40$  K/s and duration time  $-140$  s. The temperature in the reactor was measured using an optical pyrometer (Raytek, Santa Cruz, CA, USA). The catalyst support obtained by this method was called Mel/C (MW).

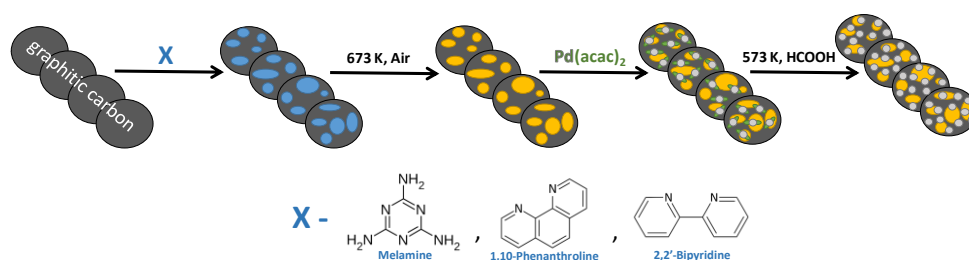


**Figure 1.** A scheme of synthesis of the catalysts based on graphitic carbon (Sibunit).

### 2.1.3. Phen/C and Bpy/C

Phenanthroline or bipyridine (Sigma-Aldrich, St. Louis, MO, USA) was dissolved in isopropyl alcohol (1 mL). The used precursor charge was selected in such a way that the deposited  $C_xN_y$ -material content in the synthesized sample was 14 wt% that was the same as for the Mel/C (muf) sample after the pyrolysis. Then, the prepared solution was added to the carbon sample and dried at 358 K. The pyrolysis was performed in the muffle furnace (673 K, 1 K/min, 2 h) in air.

### 2.2. Synthesis of Pd Catalysts

A preparation of 1 wt% Pd catalysts was performed by impregnation of the synthesized supports with a Pd acetylacetonate (Sigma-Aldrich, St. Louis, MO, USA) solution in acetone (EKOS-1, Moscow, Russia). This mixture was kept for 5 min with constant stirring followed by drying at 343 K for 1 h (Figure 1).

A preparation of a (Pd+Phen)/C catalyst was different. First, phenanthroline and  $Pd(acac)_2$ /acetone solution were mixed in attempt to obtain a complex of Pd with phenanthroline. Then this mixture was added to the Sibunit carbon. Subsequent steps were the same as above.

### 2.3. Characterization

Textural samples characteristics were determined using nitrogen adsorption-desorption on an ASAP 2400 device (Micrometrics, Norcross, GA, USA) at 77 K. The samples were pretreated in a vacuum chamber at 423 K for 1 h. The calculation of the surface area was carried out using the Brunauer-Emmett-Teller (BET) method. A CHN-analysis was performed on a Vario EL Cube element analyzer (Elementar, Langensfeld, Germany) with a thermal conductivity detector.

X-ray Diffraction (XRD) patterns were recorded using Thermo X'tra (Waltham, MA, USA) and Bruker D8 Advance (Billerica, MA, USA) diffractometers with monochromatic  $CuK\alpha$  radiation ( $\lambda = 1.5418 \text{ \AA}$ ). On the patterns, the  $2\theta$  region lower than  $15^\circ$  is not shown since the used sample holder contributed there. To measure the size of Pd particles, a high-resolution transmission electron microscopy (HRTEM) study was performed using a JEM-2100F unit (JEOL, Akishima, Japan) with the acceleration voltage of 200 kV. Determination of electronic state and surface concentrations of Pd, N, O and C was done via an AXIS Ultra DLD photoelectron spectrometer (Kratos, Manchester, UK) with monochromatic  $AlK\alpha$  radiation (1486.6 eV).  $C1s$  at 284.8 eV was chosen as the standard for energy calibration. To prevent charging of the samples the charge neutralizer was always switched on during the measurements.

### 2.4. Catalytic Measurements

Catalytic measurements were performed in a fixed-bed glass reactor attached to a catalytic flow set-up presented in Figure S1 (Supplementary Materials). Carrier gas (Ar) passed through a glass flask filled with liquid formic acid to saturate it with formic acid vapor. Then, the flow was additionally diluted with Ar until the formic acid concentration reached the value of 2.5 vol%. The total volumetric flow rate was constant and equal to 67 mL/min in all experiments. The temperature in the reactor was maintained with a furnace in the range from 323 to 673 K. The catalyst weight used in experiments corresponded to 10–16 mg. The products were analyzed by a gas chromatograph (Chromos GC-1000, Moscow, Russia) equipped with two thermal conductivity detectors and packed columns filled with CaA molecular sieves and HayeSep-Q porous polymer. For separation of the products, heating from 313 K to 483 K was performed within 10 min and then the temperature was kept stable for 20 min.

Before the measurements, the catalyst was treated with the same formic acid/Ar flow at 573 K for 20 min to decompose supported  $Pd(acac)_2$  (decomposition temperature  $\sim 478 \text{ K}$ ) and stabilize the catalyst (Figure 1). After cooling the catalyst in the formic acid/Ar flow, the measurements were started at 353 K and then performed with 15–20 K steps. The temperature was kept for 20 min at each step

to reach the steady-state. Specific reaction rates ( $W$ ) were determined basing on the Pd mass in the catalyst. They were calculated at low formic acid conversions using a formula:

$$W = \frac{X_{FA} \cdot C_{FA} \cdot v_f \cdot N_A}{22,400 \cdot m_{Pd}}, \left( \frac{\text{molecule}}{\text{s} \cdot \text{g}_{Pd}} \right) \quad (3)$$

$X_{FA}$ —formic acid conversion,  $v_f$ —total flow rate (ml/s),  $C_{FA}$ —formic acid concentration,  $m_{Pd}$ —mass of Pd in the sample (g),  $N_A$ —the Avogadro constant ( $6.02 \times 10^{23}$  molecule/mol), 22,400—volume of one mole of gas at 273 K and 1 atm (ml/mol).

### 3. Results and Discussion

#### 3.1. Characterization of the Supports

BET surface area values for the catalyst supports are shown in Table 1. They vary in a wide range from 8 m<sup>2</sup>/g to 348 m<sup>2</sup>/g for the g-C<sub>3</sub>N<sub>4</sub> and Sibunit support, respectively (Table 1). Unfortunately, the used synthesis procedure of the g-C<sub>3</sub>N<sub>4</sub> material did not provide as high surface area as that reported by Tahir et al. [26] (290 m<sup>2</sup>/g) for unknown reasons. We used different heating modes for the intermediate, but it did not allow increasing the surface area of the obtained g-C<sub>3</sub>N<sub>4</sub> material. For example, heating of the sample at 673 K for 2 h gave even a lower surface area (6.5 m<sup>2</sup>/g).

**Table 1.** Characteristics of the catalysts, supports and some kinetic data.

Sample	Support	Support Surface Area, m <sup>2</sup> /g	Mean Particle Size, nm (TEM)	E <sub>a</sub> , kJ/mol	H <sub>2</sub> Selectivity (50 % conv.) %
Pd/g-C <sub>3</sub> N <sub>4</sub>	g-C <sub>3</sub> N <sub>4</sub>	8.1	2.6 ± 0.3	39 ± 1	>98
Pd/Mel/C (muf)	Mel/C (muf)	86.5	2.0 ± 0.3	32 ± 1	>98
Pd/Mel/C (MW)	Mel/C (MW)	42.0	2.3 ± 0.5	32 ± 1	95.7
Pd/Phen/C	Phen/C	301	–	43 ± 1	90.1
(Pd + Phen)/C	C	348	–	42 ± 1	92.1
Pd/Bpy/C	Bpy/C	228	–	45 ± 1	94.8
Pd/C	C	348	2.3 ± 0.3	46 ± 2	93.4

Doping of the Sibunit surface with substances containing pyridinic nitrogen leads to a decrease of the surface area owing to occupation of the pores by the nitrogen precursor. The decrease is the strongest when melamine is used. However, the surface areas of the melamine-based supports were still high as compared to that of g-C<sub>3</sub>N<sub>4</sub> and reached 86.5 and 42 m<sup>2</sup>/g.

X-ray diffraction patterns of the g-C<sub>3</sub>N<sub>4</sub>, Mel/C, Sibunit supports and the intermediate for the carbon nitride synthesis (Inter-C<sub>x</sub>N<sub>y</sub>) are shown in Figure 2. The pattern for the intermediate shows a lot of sharp peaks, differs from the patterns presented in literature for melamine [26,30,31] and melem [32], but is very close to the pattern of melaminium nitrate [30]. Hence, we assign the Inter-C<sub>x</sub>N<sub>y</sub> intermediate to melaminium nitrate. The multiple peaks of this compound disappear after pyrolysis at 673 K. The pattern for the obtained g-C<sub>3</sub>N<sub>4</sub> sample shows only one intensive peak at 27.1° in the studied region. This peak is characteristic interplanar stacking peak for g-C<sub>3</sub>N<sub>4</sub> (JCPDS 87-1526) [33]. It indicates the presence of the ordered structure of layers of heptazine which is a monomer of g-C<sub>3</sub>N<sub>4</sub> (002 plane). Interesting that the formation of g-C<sub>3</sub>N<sub>4</sub> from melaminium nitrate takes place at the temperature lower than those from melamine reported in literature (823 K) [31,33].

Diffraction patterns of the Sibunit containing samples show diffraction peaks at 25.5° and 43.1° for the (002) and (100) planes of graphite (JCPDS 41-1487), respectively. The structure of the obtained g-C<sub>3</sub>N<sub>4</sub> is denser, as the stacking distance for the carbon nitride is by 0.2 Å smaller than that for the Sibunit carbon.

Comparing the XRD patterns for the N-containing samples with the original Sibunit sample, we conclude that g-C<sub>3</sub>N<sub>4</sub> cannot be determined using XRD because of the low carbon nitride content (12–14%) in the Mel/C sample and close positions of the g-C<sub>3</sub>N<sub>4</sub> and Sibunit characteristic peaks ((002)

plane). However, an important result is that multiple characteristic peaks of the melamine, melem or possible intermediates are absent (Figure 2). Evidently, that melamine or intermediates completely converted to supported carbon nitride or to another type of a CN containing material.

The  $C/N$  atomic ratio was determined for our  $g-C_3N_4$  support by CHN-analysis and was found to be equal to 0.63. It indicates higher nitrogen content in the sample as compared to stoichiometric  $g-C_3N_4$  (0.75). Such low ratios were reported for carbon nitrides earlier [31,34] and could be explained by the relatively low pyrolysis temperature, which we used.

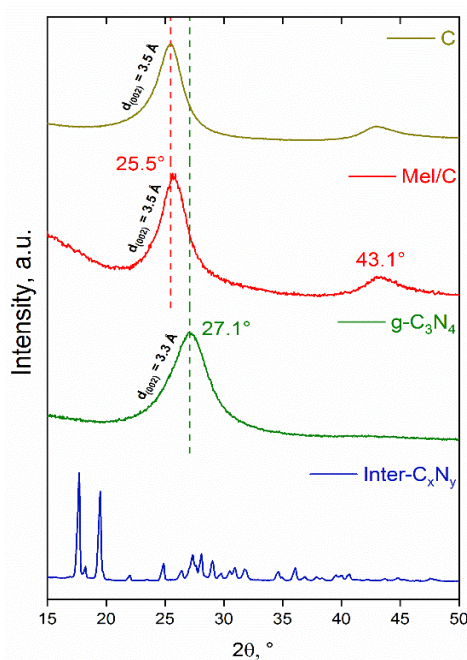


**Figure 2.** XRD patterns of the supports and intermediate of the  $g-C_3N_4$  synthesis.

### 3.2. Catalytic Activity and $H_2$ Selectivity

To elucidate the support effect, using the obtained dependences between the formic acid conversion and temperature, we calculated the reaction rates at low conversions and plotted them as the Arrhenius plots (Figure 3). It is seen that both Pd/Mel/C samples convert formic acid better than the other samples (Pd/C and Pd/ $g-C_3N_4$ ). The sample synthesized in the muffle furnace is slightly more active than the sample prepared using the microwave synthesis. However, it is worth noting that the synthesis time in the muffle furnace was 2 h, while that for the microwave synthesis was only 140 s. The difference in the rates between the melamine based Pd samples and the Pd/C sample is significant. The rates differ by a factor of 4 at about 373 K. In contrast, the Pd/ $g-C_3N_4$  sample showed the activity even lower than that for the Pd/C catalyst.

Analyzing the data presented in Figure 4, we can estimate the N-precursor effect on the catalytic activity. The catalysts prepared with bipyridine and phenanthroline show lower activities than that for the melamine-based catalyst, and they are not higher than the one of the Pd/C catalysts. These results are consistent with the data for the apparent activation energies ( $E_a$ , Table 1). The most active Pd/Mel/C catalysts show the smallest activation energy (32 kJ/mol), while the less active catalysts demonstrate higher apparent activation energies (42–46 kJ/mol). The  $E_a$  value for the Pd/ $g-C_3N_4$  catalyst is intermediate (39 kJ/mol). The difference in the apparent activation energies is significant and should be related to different properties of active sites of the catalyst. The obtained  $E_a$  values for the Pd/Mel/C catalyst are among the smallest values for formic acid decomposition over Pd catalysts in liquid and gas phase.

Important features necessary for efficient hydrogen production from formic acid are selectivity and stability. The Pd/Mel/C (muf) catalyst showed the highest selectivity (>98%) at 50% conversion (528 K) while the phenanthroline based samples showed the lowest selectivities (90–92%).

The stability of the most active Pd/Mel/C (muf) catalyst was tested for 5 h (Figure S2). In this experiment, the catalyst was not stabilized by pretreatment in the formic acid flow at 573 K as was done before other experiments. However, no significant changes of the formic acid conversion on time-on-stream was observed, and it is possible to conclude that this catalyst possesses sufficient stability to produce hydrogen from gas phase formic acid.

Hence, among the studied samples, the melamine based Pd catalysts showed the highest activity. We compared the activities of these samples with the activities of 1 wt% Ru, Pt and Au samples on the N-doped and N-free carbon supports (Table S1). This comparison showed that the metal mass-based activity of the Pd/Mel/C (muf) catalyst is slightly lower than that of the Pt/N-C catalyst, but it is higher than the activities of the other catalysts. The apparent activation energy for the melamine based Pd sample was the lowest.

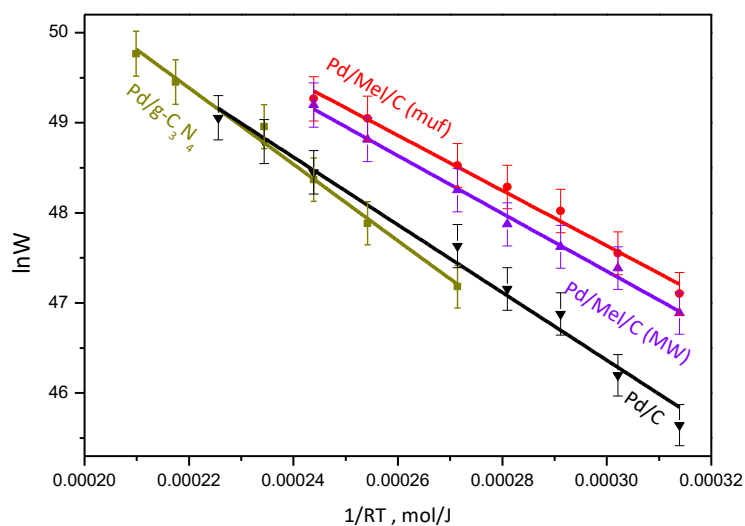


Figure 3. Arrhenius plots for formic acid decomposition showing the support effect.

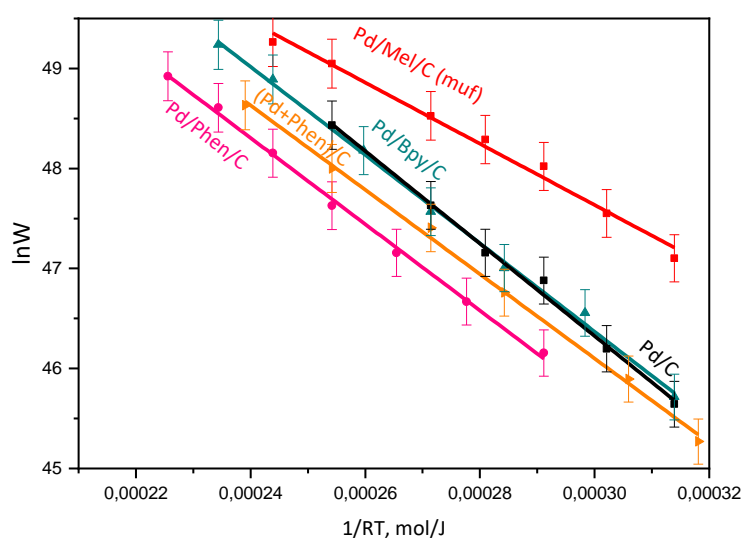
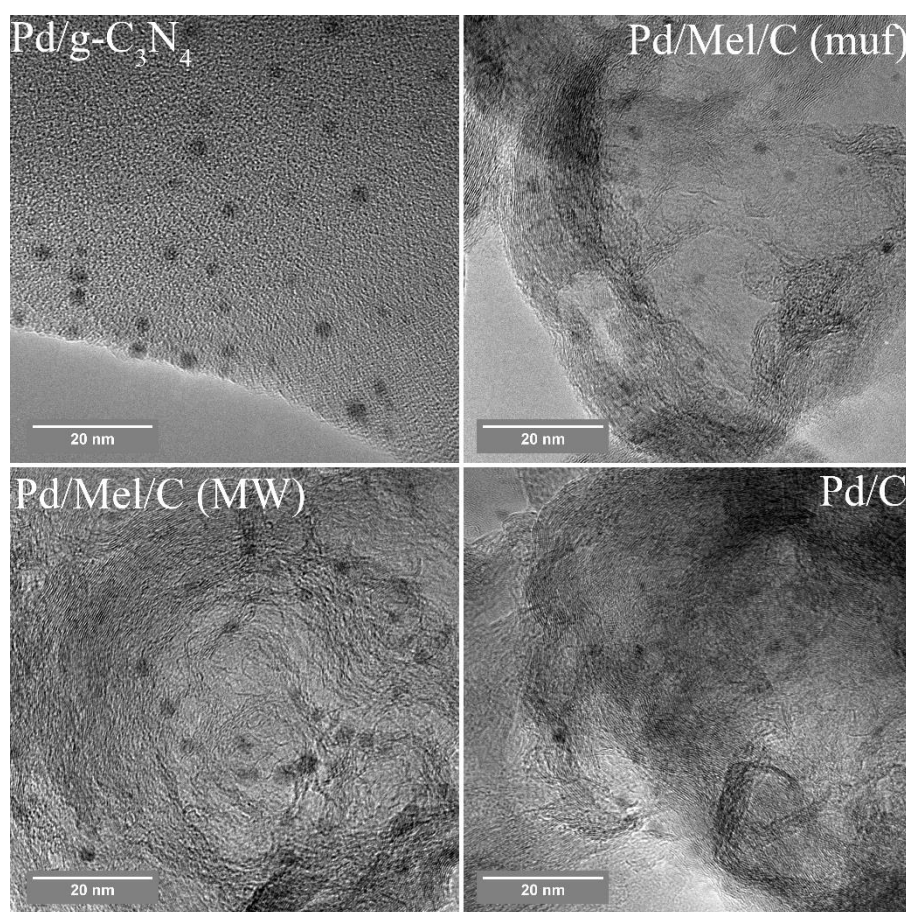


Figure 4. Arrhenius plots for formic acid decomposition showing the N-precursor effect.

### 3.3. Characterization of the Pd Catalysts

To understand the reasons of the differences in the activities of the catalysts (Figures 3 and 4) the Pd samples after the reaction were studied using HRTEM and X-ray Photoelectron spectroscopy (XPS). Figure 5 shows HRTEM images. Particle size distributions are presented in Figure S3. They are quite narrow for all studied samples indicating that the particles are rather uniform. Mean particle size data are presented in Table 1. The most active Pd/Mel/C (muf) catalyst demonstrated the smallest mean particle size (2.0 nm). An XRD study of this sample was not sensitive enough to determine Pd in this sample confirming its low content and high dispersion. The highest mean particle size was obtained for the Pd/g-C<sub>3</sub>N<sub>4</sub> sample, which corresponds to 2.6 nm. This could be related to the lowest BET surface area of the support used (Table 1). However, the mean Pd particle sizes for other two catalysts did not differ much. Generally, as it is seen in Table 1, the deposition of nitrogen precursors over the carbon surface did not provide a significant change in Pd dispersion.



**Figure 5.** HRTEM images of some catalysts after the reaction.

A C1s XP spectrum for the Pd/g-C<sub>3</sub>N<sub>4</sub> catalyst after the reaction is shown in Figure S4. It consists of two main peaks at 288.3 and 284.8 eV assigned to pyridinic (C-N=C) and adventitious carbon, respectively. The presence of the first peak confirms the formation of g-C<sub>3</sub>N<sub>4</sub>, as it is typical for this compound [26,33]. The C1s spectra for other catalysts did not differ much from each other and, hence, are not demonstrated.

N1s XP spectra for all catalysts after the reaction are shown in Figure 6. The main lines are observed at 398.8 eV assigned to pyridinic nitrogen (C-N=C) and at 400.2 eV assigned to tertiary nitrogen (N(C)<sub>3</sub>) like those in g-C<sub>3</sub>N<sub>4</sub> [33]. A shift of the N1s pyridinic line towards higher binding energies by 0.3 eV is

observed for the Pd/Mel/C (MW) catalyst. This may indicate a stronger interaction of these species in the surface layer of this sample than in the case of the Pd/Mel/C (muf) and Pd/g-C<sub>3</sub>N<sub>4</sub> samples.

Table 2 shows the total surface N concentration determined by XPS ( $N_{\text{tot}}$ ). The highest concentration was obtained for the Pd/g-C<sub>3</sub>N<sub>4</sub> catalyst (46%) followed by the Pd/Mel/C (MW) (8.9 at %) and Pd/Mel/C (muf) (4.5 at %) catalysts. The spectra of the melamine-based samples demonstrate the presence of both N1s lines, but the ratio of pyridinic species is decreased as compared to the Pd/g-C<sub>3</sub>N<sub>4</sub> sample (Table 2). The content of pyridinic N species in the Pd/Phen/C sample is negligible and Pd/Bpy/C and (Pd+Phen)/C samples do not contain pyridinic nitrogen at all. This shows that the pyridinic species have been converted either to tertiary N species or to gas products during the pyrolysis. The difference in the spectra of the melamine based and phenanthroline/bipyridine based samples can be explained at least partly by a much lower content of nitrogen in the bipyridine and phenanthroline precursors as compared to melamine (Figure 1). Generally, the state of the deposited N-containing layer in the supported samples differs from that in the g-C<sub>3</sub>N<sub>4</sub> sample. This can affect the state of supported Pd and provide the observed difference in catalytic properties (Figures 3 and 4). Therefore, the electronic state of Pd was also studied by XPS.

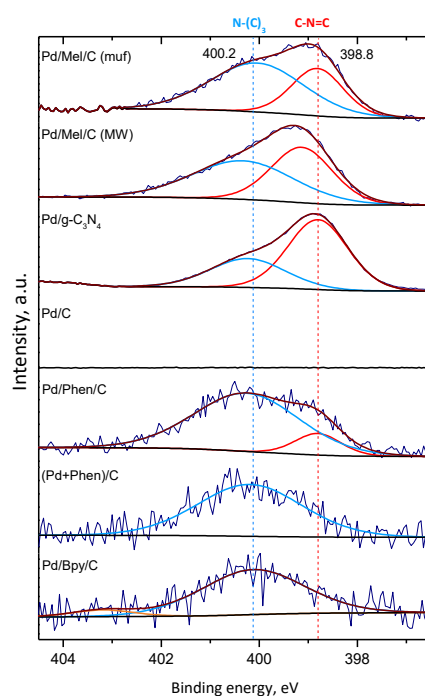


Figure 6. XP spectra of the N1s region for the catalysts after the reaction.

Table 2. Surface concentrations of N species in the catalysts after the reaction (XPS data).

Sample	Pd/g-C <sub>3</sub> N <sub>4</sub>	Pd/Mel/C (muf)	Pd/Mel/C (MW)	Pd/Phen/C	(Pd+Phen)/C	Pd/Bpy/C	Pd/C
$N_{\text{tot}}$ , at %	46.0	4.5	8.9	1.35	0.57	0.48	0
$\frac{C-N=C}{N_{\text{tot}}}$	0.66	0.35	0.46	0.14	0	0	–

Pd3d XP spectra are shown in Figure 7. The spectra consist of two components: one with Pd3d<sup>5/2</sup> at 335.0–336.4 eV (Pd3d<sup>3/2</sup> at 340.3–341.7 eV) and another with Pd3d<sup>5/2</sup> at 336.9–338.5 eV (Pd3d<sup>3/2</sup> at 342.2–343.7 eV). Taking into account the HRTEM data (Figure 5) similar for all samples, we attribute the first component to metallic Pd (Pd<sup>0</sup>), and the second component—to oxidized Pd (Pd<sup>2+</sup>). The latter can exist as a surface oxide over Pd particles. It is formed due to oxidation of the metallic Pd surface by atmospheric oxygen. Alternatively, some Pd<sup>2+</sup> species may exist in atomically dispersed state strongly

interacting with nitrogen, oxygen or carbon defects of the support [13–15,35,36]. This Pd could not be observed by the HRTEM equipment used in this work.

The Pd3d<sub>5/2</sub> line at 335.0 eV is observed for the Pd/g-C<sub>3</sub>N<sub>4</sub> catalyst, which is close to the Pd state in the unsupported bulk metal, for example, in Pd foil. The closeness of the electronic state of Pd in the sample to the Pd metal may indicate that there is no strong interaction of this Pd with the support. This can be due to small support surface area and low concentration of support sites, which can strongly interact with Pd. The lowest value of the Pd3d<sub>5/2</sub> binding energy among the Sibunit-containing catalysts is observed for the Pd/C catalyst and corresponds to 335.8 eV. This Pd state is usually attributed to small metal particles interacting with the carbon support [13,35,37]. The Pd3d<sub>5/2</sub> lines for the Pd/Mel/C (muf) and Pd/Mel/C (MW) catalysts are strongly shifted to higher binding energies (336.4 and 336.3 eV, respectively) as compared to that for the Pd/C sample. This cannot be assigned to sample charging and indicates an electron-deficient state of Pd in these samples due to a strong interaction with the support. These catalysts showed the highest activity in the formic acid decomposition reaction and the lowest values of apparent activation energies (Table 1). For the phenanthroline and bipyridine-based samples, the Pd3d<sub>5/2</sub> line positions (336.0 eV) are close to that for the Pd/C sample. The catalytic properties of these systems are also close (Figure 4).

It is an interesting question whether the Pd3d<sub>5/2</sub> line in the 336.3–336.4 eV region for the melamine-based samples can be assigned to Pd oxide (PdO). We believe that it cannot, because the Pd3d<sub>5/2</sub> binding energy for the PdO is normally located at a higher binding energy (336.8 eV) [38,39] like those observed for the Pd/g-C<sub>3</sub>N<sub>4</sub> and Pd/C samples. However, we will perform soon the necessary experiments allowing to discriminate whether the high binding energies for the Pd3d<sub>5/2</sub> line (336.3–336.4 eV) should be assigned to Pd metal or to Pd oxide by performing XPS measurements after the pretreatment of the samples in H<sub>2</sub> in the pretreatment chamber of the XP spectrometer, as it was done in some of our previous works [10,13,14]. This pretreatment easily transforms the Pd oxide into metallic Pd.

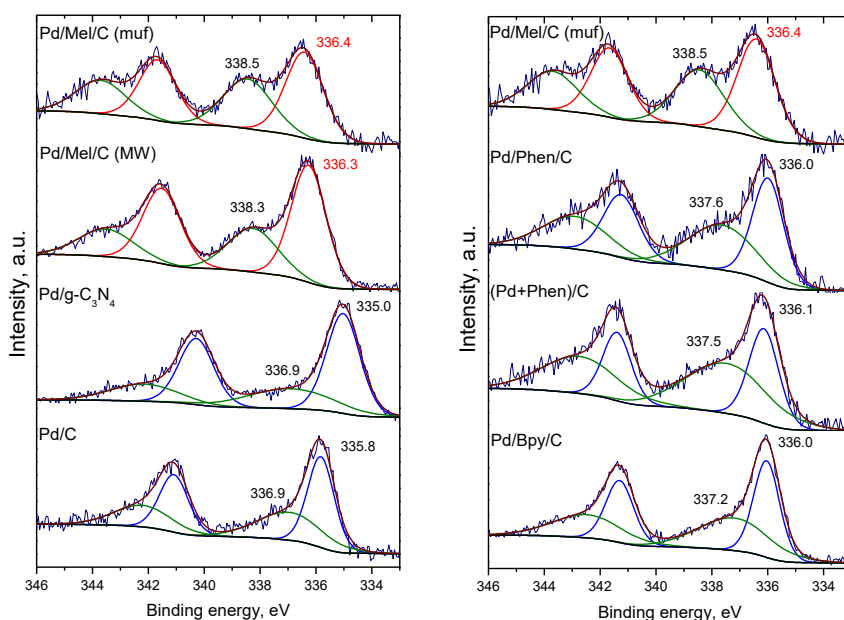


Figure 7. Pd3d XP spectra for the catalysts after the reaction.

Hence, utilization of HRTEM and XPS for the catalysts allowed explaining the effects observed for the catalytic reaction. The obtained data demonstrated that when pyridinic nitrogen exists on the surface, Pd becomes electron-deficient and the highest catalytic activity was obtained. At the same time, the presence of only tertiary nitrogen species does not positively affect the reaction.

#### 4. Conclusions

In order to obtain a high surface area N-doped support, N-containing precursors (melamine, phenanthroline or bipyridine) were deposited on the mesoporous graphitic carbon material (Sibunit) and pyrolysis at 673 K was performed. Melamine showed itself as the most promising N-precursor. The high activity of the melamine based catalysts in the hydrogen production from formic acid can be explained by a strong interaction between highly dispersed Pd nanoparticles (~2 nm) and excess of pyridinic nitrogen of the support that can bind Pd particles and provide a shift of electron density from the Pd to the support, thus, transforming Pd into an electron-deficient state. This state demonstrates a significantly enhanced catalytic activity (by a factor of 4 at 373 K), high stability in the reaction (5 h) and the lowest apparent activation energy (32 kJ/mol) as compared to the state of Pd in the other carbon supported catalysts (42–46 kJ/mol).

The used approach for synthesis of the N-doped carbon with melamine is much simpler and, if necessary, it gives a higher yield of the N-doped carbon support as compared to the direct catalytic CVD approaches. Additionally, since the used carbon support (Sibunit) was specifically developed to have high surface area and high mechanical strength, our supported Pd catalysts possessed very much the same properties. Hence, the melamine based Pd catalysts are promising for the hydrogen production from formic acid and also, probably, from other liquid organic hydrogen carriers.

**Supplementary Materials:** The following are available online at <http://www.mdpi.com/1996-1073/12/20/3885/s1>, Figure S1: Scheme of a catalytic set-up, Figure S2: Stability test for the most active catalyst. Figure S3: Particle size distributions for some catalysts after the reaction, Figure S4: C1s XP spectrum of the Pd/g-C<sub>3</sub>N<sub>4</sub> catalyst after the reaction.

**Author Contributions:** Synthesis, measurements and writing, F.S.G. and V.A.B.; characterization, S.B.; equipment creation, A.V.G.; funding security and content editing, V.N.P.; methodology, data analysis and writing, D.A.B.

**Funding:** The work was supported by the Russian Science Foundation (grant 17-73-30032).

**Acknowledgments:** The authors thank O.A. Bulavchenko for XRD measurements.

**Conflicts of Interest:** The authors declare no conflict of interest.

#### References

1. US Energy Information Administration. International Energy Outlook 2016. 2016; No. 0484. Available online: [www.eia.gov/outlooks/ieo/pdf/0484\(2016\).pdf](http://www.eia.gov/outlooks/ieo/pdf/0484(2016).pdf) (accessed on 14 October 2019).
2. Zhong, H.; Iguchi, M.; Chatterjee, M.; Himeda, Y.; Xu, Q.; Kawanami, H. Formic Acid-Based Liquid Organic Hydrogen Carrier System with Heterogeneous Catalysts. *Adv. Sust. Syst.* **2018**, *2*, 1700161. [CrossRef]
3. Boddien, A.; Federsel, C.; Sponholz, P.; Mellmann, D.; Jackstell, R.; Junge, H.; Laurenczy, G.; Beller, M. Towards the Development of a Hydrogen Battery. *Energy Environ. Sci.* **2012**, *5*, 8907–8911. [CrossRef]
4. Bulushev, D.A.; Ross, J.R.H. Towards Sustainable Production of Formic Acid. *ChemSusChem* **2018**, *11*, 821–836. [CrossRef] [PubMed]
5. Reichert, J.; Brunner, B.; Jess, A.; Wasserscheid, P.; Albert, J. Biomass Oxidation to Formic Acid in Aqueous Media Using Polyoxometalate Catalysts—Boosting Fa Selectivity by in-Situ Extraction. *Energy Environ. Sci.* **2015**, *8*, 2985–2990. [CrossRef]
6. Bulushev, D.A.; Ross, J.R.H. Heterogeneous Catalysts for Hydrogenation of CO<sub>2</sub> and Bicarbonates to Formic Acid and Formates. *Catal. Rev.* **2018**, *60*, 566–593. [CrossRef]
7. Germain, J.; Hradil, J.; Fréchet, J.M.J.; Svec, F. High Surface Area Nanoporous Polymers for Reversible Hydrogen Storage. *Chem. Mater.* **2006**, *18*, 4430–4435. [CrossRef]
8. Hull, J.F.; Himeda, Y.; Wang, W.-H.; Hashiguchi, B.; Periana, R.; Szalda, D.J.; Muckerman, J.T.; Fujita, E. Reversible Hydrogen Storage Using CO<sub>2</sub> and a Proton-Switchable Iridium Catalyst in Aqueous Media under Mild Temperatures and Pressures. *Nat. Chem.* **2012**, *4*, 383–388. [CrossRef]
9. Koroteev, V.O.; Bulushev, D.A.; Chuvilin, A.L.; Okotrub, A.V.; Bulusheva, L.G. Nanometer-Sized MoS<sub>2</sub> Clusters on Graphene Flakes for Catalytic Formic Acid Decomposition. *ACS Catal.* **2014**, *4*, 3950–3956. [CrossRef]

10. Bulushev, D.A.; Chuvilin, A.L.; Sobolev, V.I.; Stolyarova, S.G.; Shubin, Y.V.; Asanov, I.P.; Ishchenko, A.V.; Magnani, G.; Riccò, M.; Okotrub, A.V.; et al. Copper on Carbon Materials: Stabilization by Nitrogen Doping. *J. Mat. Chem. A* **2017**, *5*, 10574–10583. [CrossRef]
11. Wang, Q.; Tsumori, N.; Kitta, M.; Xu, Q. Fast Dehydrogenation of Formic Acid over Palladium Nanoparticles Immobilized in Nitrogen-Doped Hierarchically Porous Carbon. *ACS Catal.* **2018**, *8*, 12041–12045. [CrossRef]
12. Navlani-García, M.; Mori, K.; Salinas-Torres, D.; Kuwahara, Y.; Yamashita, H. New Approaches toward the Hydrogen Production from Formic Acid Dehydrogenation over Pd-Based Heterogeneous Catalysts. *Front. Mat.* **2019**, *6*. [CrossRef]
13. Podyacheva, O.; Bulushev, D.; Suboch, A.; Svintsitskiy, D.; Lisitsyn, A.; Modin, E.; Chuvilin, A.; Gerasimov, E.; Sobolev, V.; Parmon, V. Highly Stable Single-Atom Catalyst with Ionic Pd Active Sites Supported on N-Doped Carbon Nanotubes for Formic Acid Decomposition. *ChemSusChem* **2018**, *11*, 3724–3727. [CrossRef] [PubMed]
14. Zacharska, M.; Bulusheva, L.G.; Lisitsyn, A.S.; Beloshapkin, S.; Guo, Y.; Chuvilin, A.L.; Shlyakhova, E.V.; Podyacheva, O.Y.; Leahy, J.J.; Okotrub, A.V.; et al. Factors Influencing the Performance of Pd/C Catalysts in the Green Production of Hydrogen from Formic Acid. *ChemSusChem* **2017**, *10*, 720–730. [CrossRef] [PubMed]
15. Bulushev, D.A.; Zacharska, M.; Shlyakhova, E.V.; Chuvilin, A.L.; Guo, Y.; Beloshapkin, S.; Okotrub, A.V.; Bulusheva, L.G. Single Isolated Pd<sup>2+</sup> Cations Supported on N-Doped Carbon as Active Sites for Hydrogen Production from Formic Acid Decomposition. *ACS Catal.* **2016**, *6*, 681–691. [CrossRef]
16. Arrigo, R.; Hävecker, M.; Wrabetz, S.; Blume, R.; Lerch, M.; McGregor, J.; Parrott, E.P.J.; Zeitler, J.A.; Gladden, L.F.; Knop-Gericke, A.; et al. Tuning the Acid/Base Properties of Nanocarbons by Functionalization Via Amination. *J. Am. Chem. Soc.* **2010**, *132*, 9616–9630. [CrossRef]
17. Bulushev, D.A.; Sobolev, V.I.; Pirutko, L.V.; Starostina, A.V.; Asanov, I.P.; Modin, E.; Chuvilin, A.L.; Gupta, N.; Okotrub, A.V.; Bulusheva, L.G. Hydrogen Production from Formic Acid over Au Catalysts Supported on Carbon: Comparison with Au Catalysts Supported on SiO<sub>2</sub> and Al<sub>2</sub>O<sub>3</sub>. *Catalysts* **2019**, *9*, 376. [CrossRef]
18. Bi, Q.-Y.; Lin, J.-D.; Liu, Y.-M.; He, H.-Y.; Huang, F.-Q.; Cao, Y. Dehydrogenation of Formic Acid at Room Temperature: Boosting Palladium Nanoparticle Efficiency by Coupling with Pyridinic-Nitrogen-Doped Carbon. *Angew. Chem. Int. Ed.* **2016**, *55*, 11849–11853. [CrossRef]
19. Li, Z.; Li, J.; Liu, J.; Zhao, Z.; Xia, C.; Li, F. Palladium Nanoparticles Supported on Nitrogen-Functionalized Active Carbon: A Stable and Highly Efficient Catalyst for the Selective Hydrogenation of Nitroarenes. *ChemCatChem* **2014**, *6*, 1333–1339. [CrossRef]
20. Gribov, E.N.; Kuznetsov, A.N.; Golovin, V.A.; Krasnikov, D.V.; Kuznetsov, V.L. Effect of Modification of Multi-Walled Carbon Nanotubes with Nitrogen-Containing Polymers on the Electrochemical Performance of Pt/CNT Catalysts in PEMFC. *Mater. Renew. Sustain. Energy* **2019**, *8*, 7. [CrossRef]
21. Salinas-Torres, D.; Navlani-García, M.; Mori, K.; Kuwahara, Y.; Yamashita, H. Nitrogen-Doped Carbon Materials as a Promising Platform toward the Efficient Catalysis for Hydrogen Generation. *Appl. Catal. A* **2018**, *571*, 25–41. [CrossRef]
22. Cai, J.; Bennici, S.; Shen, J.; Auroux, A. Influence of N Addition in Mesoporous Carbons Used as Supports of Pt, Pd and Ru for Toluene Hydrogenation and Iron Oxide for Benzene Oxidation. *React. Kinet. Mech. Catal.* **2015**, *115*, 263–282. [CrossRef]
23. Bulushev, D.A.; Zacharska, M.; Lisitsyn, A.S.; Podyacheva, O.Y.; Hage, F.S.; Ramasse, Q.M.; Bangert, U.; Bulusheva, L.G. Single Atoms of Pt-Group Metals Stabilized by N-Doped Carbon Nanofibers for Efficient Hydrogen Production from Formic Acid. *ACS Catal.* **2016**, *6*, 3442–3451. [CrossRef]
24. Lee, J.H.; Ryu, J.; Kim, J.Y.; Nam, S.W.; Han, J.H.; Lim, T.H.; Gautam, S.; Chae, K.H.; Yoon, C.W. Carbon Dioxide Mediated, Reversible Chemical Hydrogen Storage Using a Pd Nanocatalyst Supported on Mesoporous Graphitic Carbon Nitride. *J. Mater. Chem. A* **2014**, *2*, 9490–9495. [CrossRef]
25. Oh, T.H. A Formic Acid Hydrogen Generator Using Pd/C<sub>3</sub>N<sub>4</sub> Catalyst for Mobile Proton Exchange Membrane Fuel Cell Systems. *Energy* **2016**, *112*, 679–685. [CrossRef]
26. Tahir, M.; Cao, C.; Butt, F.K.; Butt, S.; Idrees, F.; Ali, Z.; Aslam, I.; Tanveer, M.; Mahmood, A.; Mahmood, N. Large Scale Production of Novel G-C<sub>3</sub>N<sub>4</sub> Micro Strings with High Surface Area and Versatile Photodegradation Ability. *CrystEngComm* **2014**, *16*, 1825–1830. [CrossRef]
27. Material Safety Data Sheet. Melamine. Available online: <https://fscimage.fishersci.com/msds/96668.htm> (accessed on 14 October 2019).
28. Fenelonov, V.B.; Likholobov, V.A.; Derevyankin, A.Y.; Mel'gunov, M.S. Porous Carbon Materials Prepared from C<sub>1</sub>–C<sub>3</sub> Hydrocarbons. *Catal. Today* **1998**, *42*, 341–345. [CrossRef]

29. Chernousov, Y.D.; Shebolaev, I.V.; Ivannikov, V.I.; Ikryanov, I.M.; Bolotov, V.A.; Tanashev, Y.Y. An Apparatus for Performing Chemical Reactions under Microwave Heating of Reagents. *Instrum. Exp. Tech.* **2019**, *62*, 289–294. [[CrossRef](#)]
30. Vella-Zarb, L.; Braga, D.; Orpen, A.G.; Baisch, U. The Influence of Hydrogen Bonding on the Planar Arrangement of Melamine in Crystal Structures of Its Solvates, Cocrystals and Salts. *CrystEngComm* **2014**, *16*, 8147–8159. [[CrossRef](#)]
31. Papailias, I.; Giannakopoulou, T.; Todorova, N.; Demotikali, D.; Vaimakis, T.; Trapalis, C. Effect of Processing Temperature on Structure and Photocatalytic Properties of G-C<sub>3</sub>N<sub>4</sub>. *Appl. Surf. Sci.* **2015**, *358*, 278–286. [[CrossRef](#)]
32. Li, Y.; Wang, Z.; Xia, T.; Ju, H.; Zhang, K.; Long, R.; Xu, Q.; Wang, C.; Song, L.; Zhu, J.; et al. Implementing Metal-to-Ligand Charge Transfer in Organic Semiconductor for Improved Visible-near-Infrared Photocatalysis. *Adv. Mater.* **2016**, *28*, 6959–6965. [[CrossRef](#)]
33. Thomas, A.; Fischer, A.; Goettmann, F.; Antonietti, M.; Müller, J.-O.; Schlögl, R.; Carlsson, J.M. Graphitic Carbon Nitride Materials: Variation of Structure and Morphology and Their Use as Metal-Free Catalysts. *J. Mater. Chem.* **2008**, *18*, 4893–4908. [[CrossRef](#)]
34. Vorobyeva, E.; Chen, Z.; Mitchell, S.; Leary, R.K.; Midgley, P.; Thomas, J.M.; Hauert, R.; Fako, E.; Lopez, N.; Perez-Ramirez, J. Tailoring the Framework Composition of Carbon Nitride to Improve the Catalytic Efficiency of the Stabilised Palladium Atoms. *J. Mater. Chem. A* **2017**, *5*, 16393–16403. [[CrossRef](#)]
35. Chesnokov, V.V.; Kriventsov, V.V.; Malykhin, S.E.; Svintsitskiy, D.A.; Podyacheva, O.Y.; Lisitsyn, A.S.; Richards, R.M. Nature of Active Palladium Sites on Nitrogen Doped Carbon Nanofibers in Selective Hydrogenation of Acetylene. *Diam. Relat. Mater.* **2018**, *89*, 67–73. [[CrossRef](#)]
36. Arrigo, R.; Schuster, M.E.; Xie, Z.; Yi, Y.; Wowsnick, G.; Sun, L.L.; Hermann, K.E.; Friedrich, M.; Kast, P.; Hävecker, M.; et al. Nature of the N–Pd Interaction in Nitrogen-Doped Carbon Nanotube Catalysts. *ACS Catal.* **2015**, *5*, 2740–2753. [[CrossRef](#)]
37. Stonkus, O.A.; Kibis, L.S.; Yu. Podyacheva, O.; Slavinskaya, E.M.; Zaikovskii, V.I.; Hassan, A.H.; Hampel, S.; Leonhardt, A.; Ismagilov, Z.R.; Noskov, A.S.; et al. Palladium Nanoparticles Supported on Nitrogen-Doped Carbon Nanofibers: Synthesis, Microstructure, Catalytic Properties, and Self-Sustained Oscillation Phenomena in Carbon Monoxide Oxidation. *ChemCatChem* **2014**, *6*, 2115–2128. [[CrossRef](#)]
38. Brun, M.; Berthet, A.; Bertolini, J.C. XPS, AES and Auger Parameter of Pd and PdO. *J. Electron Spectrosc. Relat. Phenom.* **1999**, *104*, 55–60. [[CrossRef](#)]
39. Kibis, L.S.; Titkov, A.I.; Stadnichenko, A.I.; Koscheev, S.V.; Boronin, A.I. X-ray Photoelectron Spectroscopy Study of Pd Oxidation by RF Discharge in Oxygen. *Appl. Surf. Sci.* **2009**, *255*, 9248–9254. [[CrossRef](#)]



© 2019 by the authors. Licensee MDPI, Basel, Switzerland. This article is an open access article distributed under the terms and conditions of the Creative Commons Attribution (CC BY) license (<http://creativecommons.org/licenses/by/4.0/>).